GEOPHYSICAL RESEARCH LETTERS, VOL. 33, L15302, doi:10.1029/2006GL026734, 2006

Using uplifted Holocene beach berms for paleoseismic analysis on the Santa María Island, south-central Chile

B. Bookhagen,[1,2] H. P. Echtler,[3] D. Melnick,[3,4] M. R. Strecker,[1] and J. Q. G. Spencer[5,6]

Received 28 April 2006; revised 29 May 2006; accepted 7 June 2006; published 2 August 2006.

[1] Major earthquakes (M > 8) have repeatedly ruptured the Nazca-South America plate interface of south-central Chile involving meter scale land-level changes. Earthquake recurrence intervals, however, extending beyond limited historical records are virtually unknown, but would provide crucial data on the tectonic behavior of forearcs. We analyzed the spatiotemporal pattern of Holocene earthquakes on Santa María Island (SMI; 37°S), located 20 km off the Chilean coast and approximately 70 km east of the trench. SMI hosts a minimum of 21 uplifted beach berms, of which a subset were dated to calculate a mean uplift rate of 2.3 ± 0.2 m/ky and a tilting rate of 0.022 ± 0.002 °/ky. The inferred recurrence interval of strandline-forming earthquakes is ~180 years. Combining coseismic uplift and aseismic subsidence during an earthquake cycle, the net gain in strandline elevation in this environment is ~0.4 m per event. **Citation:** Bookhagen, B., H. P. Echtler, D. Melnick, M. R. Strecker, and J. Q. G. Spencer (2006), Using uplifted Holocene beach berms for paleoseismic analysis on the Santa María Island, south-central Chile, *Geophys. Res. Lett.*, *33*, L15302, doi:10.1029/2006GL026734.

1. Introduction

[2] The geomorphology and depositional record of the tectonically active continental margin of Chile reflect regional uplift and subsidence associated with large subduction earthquakes [e.g., *Darwin*, 1851; *Plafker and Savage*, 1970; *Thatcher*, 1989]. Tectonic deformation on timescales of 10^5 to 10^6 years has resulted in distinct seismotectonic segments along the forearc, often characterized by staircase marine abrasion platforms. Such marine terraces are valuable recorders of coastal tectonic activity and may aid in identifying differential uplift and tilting rates [e.g., *Kaizuka et al.*, 1973; *Marquardt et al.*, 2004; *Melnick et al.*, 2006; *Radtke*, 1987; *Schellmann and Radtke*, 2003]. However, while these terraces record the complex interplay between long-term tectonic uplift rate and superposed glacio-eustatic sea-level changes [e.g., *Bloom*, 1998; *Pinter et al.*, 1998; *Taylor et al.*, 1987] they do not allow earthquake cycles to be identified. In contrast, historic earthquake records along the Chilean coast permit single events to be deciphered, but these records only span the last five hundred years – a timescale often not sufficiently long enough for reliable recurrence-interval calculations. It is thus difficult to combine the information provided by both types of records and use them to assess the tectonic behavior of coastal segments on timescales spanning $\sim 10^2$ to 10^3 years.

[3] In an effort to reconstruct paleoseismicity in coastal environments, precise information is needed on the amount of uplift during each earthquake, integrated over instantaneous, coseismic uplift and protracted, interseismic subsidence. The amount of coseismic uplift during recent earthquakes has ranged between decimeters and several meters, but the degree of post-seismic relaxation and associated subsidence are poorly constrained [*Chlieh et al.*, 2004; *Darwin*, 1851; *Lomnitz*, 2004; *Plafker*, 1972]. There is thus a need for better constraining the short-term deformation and uplift history of the Chilean coast. In order to bridge the gap between historic and long-term uplift records in this environment, we analyzed Holocene emerged beach berms that provide valuable insight into the history of major subduction-zone earthquakes, coeval uplift, and interseismic subsidence. Unlike Pleistocene marine terraces, Holocene beach berms are either recorders of paleoearthquakes or varying storm activity, because Holocene sea level has not been oscillating [*Siddall et al.*, 2003]. We mapped, surveyed, and dated beach berms on Santa María Island, south central Chile, to decipher paleoseismic activity, recurrence intervals, and land-level changes during several earthquake cycles.

2. Setting, Approach, and Methods

[4] The tectonically active coast of Chile is an integral part of the convergence zone between the oceanic Nazca plate and South American continent. The Nazca plate is subducted at a present-day rate of 66 mm/y [*Angermann et al.*, 1999; *Stein et al.*, 1986]. Long-term geological convergence estimates for the past ~3 My are ~80 mm/y [*Somoza*, 1998]. Interaction between the subducting Nazca and the overriding South American plates has led to differential coastal uplift and faulting that ultimately define distinct seismotectonic segments. Here, we focus on Santa María Island (SMI), located in the southern Concepción seismotectonic segments [e.g., *Barrientos et al.*, 1992; *Beck et al.*, 1998; *Comte et al.*, 1986; *Lomnitz*, 2004; *Melnick et al.*, 2006]. The SMI is located at 37°S, about 75 km east of the Chile trench (Figure 1a). It is situated above an east-vergent blind reverse-fault system, apparently rooted in the plate interface, and inferred to rupture during large subduction

[1]Institut für Geowissenschaften, Universität Potsdam, Potsdam, Germany.
[2]Now at Geological and Environmental Sciences, Stanford University, Stanford, California, USA.
[3]GeoForschungsZentrum Potsdam, Telegrafenberg, Potsdam, Germany.
[4]Also at Institut für Geowissenschaften, Universität Potsdam, Potsdam, Germany.
[5]School of Geography and Geosciences, University of St Andrews, St. Andrews, UK.
[6]Now at Institut für Geologie und Paläontologie, Universität Innsbruck, Innsbruck, Austria.

0094-8276/06/2006GL026734$05.00

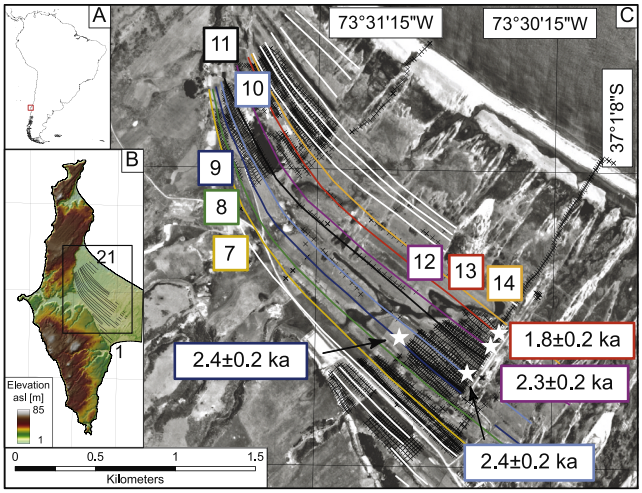

Figure 1. Airphoto of lower-elevation part of the Santa María Island (SMI). Beach-berm crests are outlined in color and laser total-station measurements (>8000) are shown by black crosses. (a) Location of study site and (b) the high-resolution digital elevation model for the SMI.

zone earthquakes [*Melnick et al.*, 2006]. Uplift of the SMI is not influenced by post-glacial rebound as Pleistocene glaciation at this latitude was confined to the Main Cordillera (>2 km), roughly 200 km east of the island [e.g., *Rabassa and Clapperton*, 1990].

[5] The island comprises a tilted Pleistocene upper surface and adjacent lowlands dominated by emerged Holocene strandlines (Figure 1b). The tilted surface is formed by Tertiary sediments that are unconformably overlain by the late Pleistocene Santa María Formation. Based on geomorphic mapping and interpretation of seismic reflection profiles, the overall asymmetric shape of this surface has been linked to underlying blind reverse faults [*Melnick et al.*, 2006]. The lowlands are characterized by well preserved beach berms in an elevation range between 0.5 to 8 m amsl (above mean sea level) that record ongoing tectonic uplift.

[6] We identified a total of 21 beach berms, of which 15 are well preserved, while an additional 6 berms have been modified by aeolian and anthropogenic influence. In order to quantify the deformation field of the uplifted berms, we surveyed parallel and perpendicular to their paired crests and low-lying parts with a laser-total station. We measured beach-berm topography along berm tops, mid slope, and beach face and recorded more than 8000 elevation points with sub-centimeter accuracy to identify geomorphic features on 10^{-1} to 10^{3} m length scales.

[7] The evolution of the 0.5 to 1-m-high beach berms is complex, as marine, aeolian and tectonic processes may interact during their formation [e.g., *Carter*, 1986; *Reineck and Singh*, 1980]. Berms are shore-parallel linear sediment bodies of triangular cross section with a horizontal to gently landward dipping surface (berm top), and a steeper seaward-dipping slope (beach face). A berm forms during intense winter storms when high-energetic waves deposit sand and silt onshore [e.g., *Carter*, 1986]. On SMI, the active beach berm is located ~30 m from the shoreline, within 0.5 m of mean tidal sea level, and its crest has a constant elevation along the shore. In order to understand the significance of these deposits and make use of their tectono-geomorphic potential, it is important to emphasize that the uplifted berms are identical to their modern counterparts. Uplifted berms thus document the former intersection between sea level and the emerging island. This is corroborated by the following observations: (1) paleo-beach berms run strictly parallel to each other, and mimic higher, upward topography of the Pleistocene units, representing the cliff of a paleo-shoreline, (2) the slightly elevated crests of the paleo-beach berms have coarser grain sizes than present-day aeolian or fluvial deposits, (3) the deposits have no aeolian cross or laminar bedding features, and (4) all of the low lying back-swamp sectors are characterized by clayey to silty, organic-rich soils originally formed in tidal slacks (Figure 2).

[8] Analogous to other tectonically active coasts, and historical accounts of meter-scale coseismic uplift at SMI, we infer that these beach berms record large earthquakes [e.g., *Berryman*, 1993; *Darwin*, 1851; *Echtler et al.*, 2004; *Lomnitz*, 1970, 2004; *Yamaguchi and Ota*, 2004]. Only an instantaneous, coseismically uplifting island can preserve the paleo beach berms, while a slow, aseismic-uplifting island with a nearly constant sea level most likely results in massive beach deposits. Furthermore, we posit that the berms represent a continuous earthquake record: The berms extend for several kilometers across a differentially uplifting zone. Along strike in a southeast-northwest direction, the quantity, sedimentologic characteristics, and slope of the berm crests are similar, suggesting that no single berm has been eroded. Note that the horizontal spacing of the berms is controlled by the underlying slope of the marine platform, while their vertical spacing is dominated by tectonic displacement.

[9] We dated the sandy beach berm deposits using the single-aliquot regenerative-dose (SAR) optically stimulated luminescence (OSL) method [e.g., *Aitken*, 1998]. The OSL data record the time when quartz grains became immobile and shielded from light, thus providing a minimum age for the deposits. We measured 30-40 single aliquots from each sample to assess the equivalent dose. We obtained two OSL

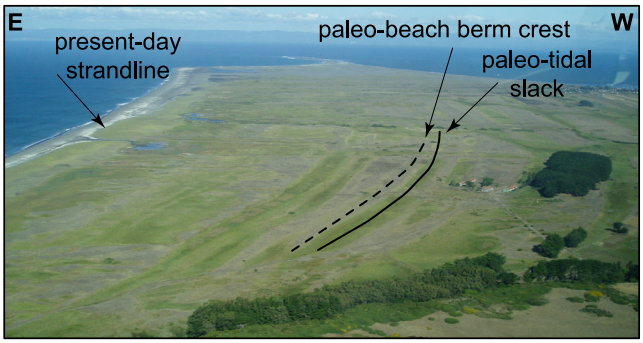

Figure 2. Aerial view to the southeast taken subparallel to the paired beach berms. Note the former tidal slacks (low-lying areas, solid black line) that support a dense green grassland vegetation, which has developed over silty organic soil with high water holding capacity. These areas contrast with higher, sandier and drier former beach crest environments (black dotted line) supporting shrubs.

Table 1. Beach Berm Numbers, Associated Optically Stimulated Luminescence (OSL) Ages, and 1-Sigma Errors (for Extended Information we Refer to Table S1)[a]

Beach Berm Numbers	Sample Depth, m	Equivalent Dose, Gy	Total-Dose Rate, $mGya^{-1}$	Age, ka	Tilt Rate, °/ky	Mean Elev., m asl	Uplift Rate, m/ky
13	0.55	3.11 ± 0.34	3.11 ± 0.04	1.8 ± 0.2	0.017 ± 0.002	3.9	2.1 ± 0.3
12	0.50	4.30 ± 2.15	4.30 ± 0.04	2.8 ± 1.4	0.019 ± 0.001	4.7	2.1 ± 0.2
12	0.55	3.57 ± 0.26	3.57 ± 0.04	2.2 ± 0.2			
10	0.50	4.47 ± 0.29	4.47 ± 0.04	2.8 ± 0.2	0.025 ± 0.002	5.6	2.4 ± 0.2
10	0.59	3.87 ± 0.26	3.87 ± 0.04	2.4 ± 0.2			
9	0.48	5.02 ± 1.30	5.02 ± 0.04	3.4 ± 0.9	0.028 ± 0.002	6.0	2.6 ± 0.2
9	0.65	3.93 ± 0.27	3.93 ± 0.04	2.3 ± 0.2			
				Average	0.022 ± 0.002		2.3 ± 0.2

[a]Equivalent dose values are mean and 1-sigma standard error; total dose-rates calculated using U, Th, K and Rb data from ICP-MS and XRF analyses that were converted to beta and gamma dose-rates, attenuated for sample water content, and summed with a calculated estimate of cosmogenic dose-rate. Tilting and uplift rates are calculated using along beach-berm elevation change and mean elevations from the southeastern part of the preserved beach berms.

samples for 3 of the 4 dated berms and inversely weighted the mean ages by the square of their errors.

3. Results

[10] We used our precise elevation measurements and OSL age data of the beach berms to (1) calculate tilting rates, (2) quantify uplift rates, (3) estimate earthquake recurrence intervals, and (4) to estimate the seismogenically increment of average elevation. We identified and surveyed 15 well-preserved beach berms, and sampled 4 paired berms for OSL dating (Table 1 and Table S1[1]). Subparallel to the present shoreline, the beach berms have been progressively tilted to the NW (Figure 3), suggesting a constant deformation mechanism. Using the obtained ages, the averaged tilting rate is 0.022 ± 0.002 °/ky (Table 1). The uplift rate appears to be nearly constant throughout the dated interval, with an averaged rate of 2.3 ± 0.2 m/ky (Table 1). While the beach berms closer to the coast are influenced by aeolian processes, linearly extrapolating over this narrow band using the distance-elevation relationship from the measured beach berms predicts the present-day shoreline at ~0.5 m elevation. We attribute this discrepancy to incomplete interseismic relaxation. This assumption is supported by the observation that the marine platform uplifted during the 1835 earthquake has remained virtually unchanged [*Darwin*, 1851; *Melnick et al.*, 2006].

[11] The calculated earthquake-recurrence interval for the well-dated time period between ~1.8 and ~2.4 ka with 4 recorded beach-berm forming events is ~150 years. The derived average-elevation gain between each beach-berm crest is 0.4 ± 0.15 m, with two significant exceptions: beach berms 11 and 13 have larger-than-average offsets of ~0.8 and ~0.6 m, respectively.

4. Discussion and Conclusion

[12] The uplifted beach berms provide a unique data set to study the deformation history of the island as an integral part of the forearc. The uniform tilting rates suggest a spatially constant differential uplift pattern throughout each earthquake cycle during mid to late Holocene time. Similarly, uplift rates have remained constant throughout the measured time interval. Interestingly, tilting and uplift-rate estimates for the Late Pleistocene yield comparable values [*Melnick et al.*, 2006], indicating a nearly continuous constant uplift history for the island, and probably the entire Concepción seismotectonic segment.

[13] In order to expand the information gained from the age dating and to assign ages to the yet undated beach berms, we exploit the measured constant uplift rate and substitute space for time. Thereby, the crest elevation between each beach berm is assigned an age with the constant uplift rate of 2.3 mm/y. This is supported by the linear relation between the distance from the active beach berm and the crest elevation (Figure 4). The averaged recurrence interval, which is now 180 ± 65 y and allows us to view the data in an extended temporal perspective (Figure 5). Historic earthquake records for the Concepción seismotectonic segment reach back to the year 1575, and six events with varying magnitudes and rupture lengths indicate a recurrence interval of 88 ± 5 years [*Lomnitz*, 1970, 2004]. Similar discrepancies between short and long-term earth-

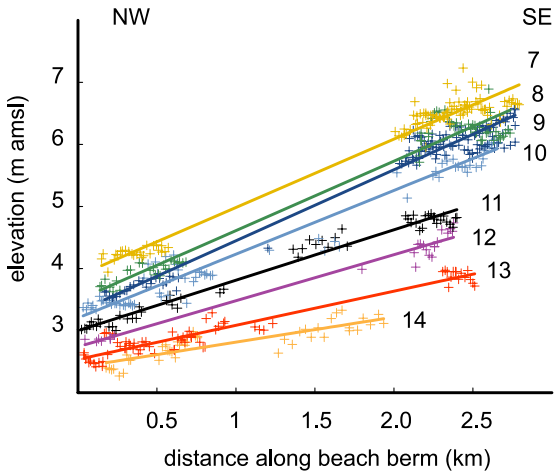

Figure 3. Distance along the beach-berm crests from northwest to southeast. The convergence of the beach berms in the NW of the island documents progressive tilting. Colors of beach crests correspond to beach berms shown in Figure 1. The solid lines represent linear fits between the berm elevations from the northwestern and southeastern parts. See Table 1 for tilt rates associated with beach-berm numbers 9, 10, 12, 13.

[1]Auxiliary materials are available in the HTML. doi:10.1029/2006GL026734.

quake recurrence intervals were observed in the southern Valdivia seismotectonic segment, where the historically recorded recurrence interval is inferred to be 128 years, whereas sedimentary evidence spanning the last 2000 years suggests a recurrence interval of 285 years [*Cisternas et al.*, 2005; *Lomnitz*, 2004]. There, sedimentological evidence from the estuary of Río Maullín was used to identify six megathrust events prior to the largest instrumentally recorded earthquake (Mw 9.5) in south-central Chile in 1960 [*Cisternas et al.*, 2005]. During this earthquake and preceding events the Río Maullín estuary and other coastal areas on the mainland experienced net uplift [*Atwater et al.*, 1992]. An independent earthquake record relating turbidites and seismic triggering from a well-dated Late Pleistocene to Holocene marine sediment core in the trench at ODP site 1232 reveals a similar earthquake frequency of ~230 years [*Blumberg et al.*, 2006]. In general, the two seismotectonic segments appear to have their own recurrence intervals in the time scales studied.

[14] Lateral, more resistant pinch-out layers, steeply dipping reverse faults and anticlines associated with seismic activity suggest that ongoing deformation on SMI is controlled by a blind reverse fault, which may be a regional feature controlling deformation in the forearc [*Melnick et al.*, 2006]. Interestingly, there appears to be no simple relationship between the amount of offset and associated recurrence interval (Figure 5), but ages are too sparse to identify a cyclic deformation behavior.

[15] On SMI the mean elevation difference between each berm crest is ~0.4 m. This corresponds to the amount of net elevation gain between each beach-berm forming earthquake (or earthquake cycle), a value integrating over coseismic uplift, interseismic subsidence, and possibly aseismic creep. Interestingly, events 11 and 13 appear to fall outside the expected relationship between earthquake and offset, with a crest difference of ~0.6 and ~0.8 m, respectively. This might correspond to larger coseismic offset in the associated earthquake events, lower postseismic relaxation, or longer interseismic strain accumulation. Our limited age control indicates that the time interval preceding these uplift events is roughly twice as long, suggesting a larger strain accumulation that is released during a larger earthquake with a higher offset.

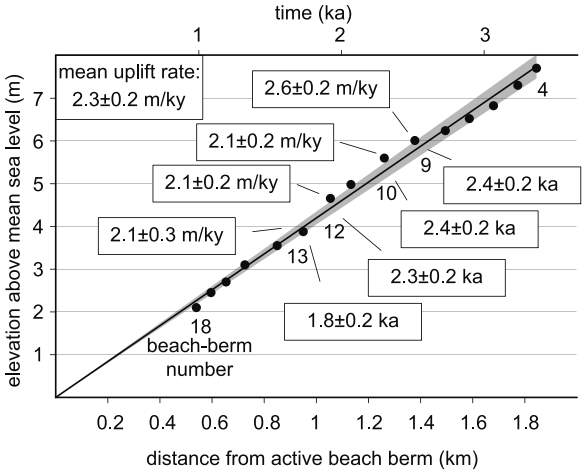

Figure 4. Linear relationship between the distance from the active beach berm at the shoreline and beach-berm crest elevations. Note the nearly constant uplift rate that allow substituting space for time and inferring ages for the undated beach berms. Gray shading indicates errors associated with age dating. The mean net elevation gain during an earthquake cycle is ~0.4 m between each beach berm. Berms # 11 and 13 are characterized by a larger offset of ~0.6 and ~0.8 m, respectively.

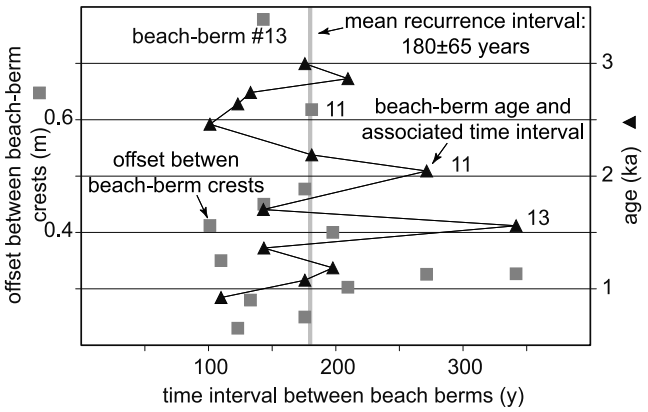

Figure 5. Inferred recurrence intervals and offset for beach-berm forming earthquakes. Note that there is no apparent relationship between the beach-berm crests offset and associated earthquake-recurrence time interval (gray squares). However, the longest time interval before earthquakes coincides with the highest offset for beach berms # 11 and 13. Triangles indicate the relationship between recurrence interval and age, while the gray bar outlines the mean recurrence interval of ~180 years.

[16] The 15 beach berms allow us to link deformation on short (10^2 y) and medium (10^3 y) timescales. The good preservation of the unique record can be attributed to (1) the steady, but fast uplift of SMI, (2) a nearly constant sea level throughout the mid to late Holocene [*Siddall et al.*, 2003], (3) the protection from strong winds through higher topography on the windward side to the southwest, and (4) the protection from wave erosion through landward beach and dune exposure. We suggest that the beach berms represent a continuous paleoseismicity record, because we do not observe erosive sedimentary processes other than those associated with beach berm formation in berm depth profiles. The change in elevation of the berm crests is thus associated with tectonic processes. Alternatively, the net-elevation gain can be related to aseismic creep associated with interseismic strain not released during coseismic events. However, this most likely would only account for a small percentage of the overall uplift, as the preservation of the beach berms is directly controlled by coseismic vertical offset raising the berms above the influence of the wave erosion.

[17] In conclusion, the uplift history of Holocene beach berms on SMI indicates constant uplift throughout the Holocene of ~2.3 mm/y and tilting of ~0.02 °/ka toward the northwest. These moderate to fast uplift rates can be used to constrain deformation within this seismotectonic segment. Our record suggests an earthquake recurrence interval of ~180 years from the mid-Holocene until today

that is approximately twice the recurrence interval derived from historic earthquake records.

[18] **Acknowledgments.** This is publication no. GEOTECH - 231 of the TIPTEQ project (from the Incoming Plate to megaThrust EarthQuakes) in the framework of the GEOTECHNOLOGIEN program funded by the German Ministry of Education and Research (BMBF) and German Research Foundation (DFG), Grant (03G0594A). We appreciate constructive reviews by D. Burbank and R. Bürgmann. M.S. acknowledges additional support by the A. Cox fund of Stanford University.

References

Aitken, M. J. (1998), *An Introduction to Optical Dating*, 267 pp., Oxford Univ. Press, New York.

Angermann, D., et al. (1999), Space-geodetic estimation of the Nazca-South America Euler vector, *Earth Planet. Sci. Lett.*, *171*, 329–334.

Atwater, B. F., et al. (1992), Net late Holocene emergence despite earthquake-induced submergence, south-central Chile, *Quat. Int.*, *15/16*, 77–85.

Barrientos, S. E., G. Plafker, and E. Lorca (1992), Postseismic coastal uplift in southern Chile, *Geophys. Res. Lett.*, *19*, 701–704.

Beck, S., et al. (1998), Source characteristics of historic earthquakes along the Central Chile subduction zone, *J. S. Am. Earth Sci.*, *11*, 115–129.

Berryman, K. (1993), Age, height, and deformation of Holocene marine terraces at Mahia Peninsula, Hikurangi subduction margin, New-Zealand, *Tectonics*, *12*, 1347–1364.

Bloom, A. L. (1998), *Geomorphology: A Systematic Analysis of Late Cenozoic Landforms*, 3rd ed., 482 pp., Prentice-Hall, Upper Saddle River, N. J.

Blumberg, S., et al. (2006), ODP site 1232 off southern Chile—An archive of late quaternary climate and tectonics (abstract), *Geophys. Res. Abstr.*, *8*, 10571.

Carter, R. W. G. (1986), The morphodynamics of beach-ridge formation—Magilligan, Northern-Ireland, *Mar. Geol.*, *73*, 191–214.

Chlieh, M., et al. (2004), Crustal deformation and fault slip during the seismic cycle in the North Chile subduction zone, from GPS and InSAR observations, *Geophys. J. Int.*, *158*, 695–711.

Cisternas, M., et al. (2005), Predecessors of the giant 1960 Chile earthquake, *Nature*, *437*, 404–407.

Comte, D., et al. (1986), The 1985 central Chile earthquake—A repeat of previous great earthquakes in the region, *Science*, *233*, 449–453.

Darwin, C. (1851), *Geological Observations on Coral Reefs*, *Volcanic Islands*, *and on South America-Being the Voyage of the Beagle*, *Under the Command of Captain Fitzroy*, *R. N.*, *During the Years 1832 to 1836*, 279 pp., Smith Elder, London.

Echtler, H. P., et al. (2004), Quaternary tectonic tilting governed by rupture segments controls surface morphology and drainage evolution along the south-central coast of Chile, *Eos Trans. AGU*, *85*(47), Fall Meet. Suppl., Abstract T13C-1389.

Kaizuka, S., et al. (1973), Quaternary tectonic and recend seismic crustal movements in the Arauco peninsula and its environs, central Chile, *Geogr. Rep. Tokyo Metrop. Univ.*, *8*, 1–38.

Lomnitz, C. (1970), Some observations of gravity waves in 1960 Chile earthquake, *Bull. Seismol. Soc. Am.*, *60*, 669–670.

Lomnitz, C. (2004), Major earthquakes of Chile: A historical survey, 1535–1960, *Seismol. Res. Lett.*, *75*, 368–378.

Marquardt, C., et al. (2004), Coastal neotectonics in southern central Andes: Uplift and deformation of marine terraces in northern Chile (27 degrees S), *Tectonophysics*, *394*, 193–219.

Melnick, D., et al. (2006), Coastal deformation and great subduction earthquakes: Santa María, Chile (37°S), *Geol. Soc. Am. Bull.*, doi:10.1130/b25865.1, in press.

Pinter, N., et al. (1998), Late quaternary slip on the Santa Cruz Island fault, California, *Geol. Soc. Am. Bull.*, *110*, 711–722.

Plafker, G. (1972), Alaskan earthquake of 1964 and Chilean earthquake of 1960—Implications for arc tectonics, *J. Geophys. Res.*, *77*, 901–925.

Plafker, G., and J. C. Savage (1970), Mechanism of Chilean earthquakes of May 21 and May 22, 1960, *Geol. Soc. Am. Bull.*, *81*, 1001–1030.

Rabassa, J., and C. M. Clapperton (1990), Quaternary glaciations of the southern Andes, *Quat. Sci. Rev.*, *9*, 153–174.

Radtke, U. (1987), Marine terraces in Chile (22°–32°S), geomorphology, chronoestratigraphy and neotectonics: Preliminary results, *Quat. S. Am. Antarct. Peninsula*, *5*, 239–256.

Reineck, H. E., and I. B. Singh (1980), *Depositional Sedimentary Environments*, 2nd ed., 551 pp., Springer, New York.

Schellmann, G., and U. Radtke (2003), Coastal terraces and Holocene sea-level changes along the Patagonian Atlantic coast, *J. Coastal Res.*, *19*, 983–996.

Siddall, M., et al. (2003), Sea-level fluctuations during the last glacial cycle, *Nature*, *423*, 853–858.

Somoza, R. (1998), Updated Nazca (Farallon)—South America relative motions during the last 40 My: Implications for mountain building in the central Andean region, *J. S. Am. Earth Sci.*, *11*, 211–215.

Stein, S., et al. (1986), The Nazca-South America convergence rate and the recurrence of the Great 1960 Chilean earthquake, *Geophys. Res. Lett.*, *13*, 713–716.

Taylor, F. W., et al. (1987), Analysis of partially emerged corals and reef terraces in the central Vanuatu Arc—Comparison of contemporary coseismic and nonseismic with quaternary vertical movements, *J. Geophys. Res.*, *92*, 4905–4933.

Thatcher, W. (1989), Earthquake recurrence and risk assessment in Circum-Pacific seismic gaps, *Nature*, *341*, 432–434.

Yamaguchi, M., and Y. Ota (2004), Tectonic interpretations of Holocene marine terraces, east coast of Coastal Range, Taiwan, *Quat. Int.*, *115*, 71–81.

B. Bookhagen, Department of Geological and Environmental Sciences, 450 Serra Mall, Braun Hall, Building 320, Stanford University, Stanford, CA 94305–2115, USA. (bodo@pangea.stanford.edu)

H. P. Echtler and D. Melnick, GeoForschungsZentrum Potsdam, Telegrafenberg, D-14473 Potsdam, Germany.

J. Q. G. Spencer, Institut für Geologie und Paläontologie, Universität Innsbruck, A-6020 Innsbruck, Austria.

M. R. Strecker, Institut für Geowissenschaften, Universität Potsdam, Postfach 60 15 53, D-14415 Potsdam, Germany.